26 Ion Beam Analysis

K.G. Malmqvist

Division of Nuclear Physics, Lund Institute of Technology at Lund University,
P.O. Box 118, 22100 Lund, Sweden
klas.malmqvist@pixe.lth.se

26.1 Introduction

The common denominator in the field of ion beam analysis (IBA) is the use of accelerated charged particles, interacting with a specimen and hence producing radiation suitable for analytical purposes. Here the definition of IBA is limited to charged particles with an initial energy of the order of MeV/u, i.e. ions produced in small and medium-size particle accelerators.

The basic mechanisms behind the IBA techniques vary significantly but all depend strongly on the ion–solid interactions occurring when a specimen is bombarded with an ion beam. The theory and physics behind the atomic collisions that govern the ion trajectories in the specimen are described in detail in Chap. 24. Many decades of careful basic physics studies of such interactions have enabled the IBA field to make use of the databases created on reaction cross sections, energy loss, energy straggling etc. [1, 2]. The well-defined ion range and almost straight ion tracks obtained when using MeV ions are utilized in the various IBA methods. The penetration depth in most materials is of the order of tens of μm, and the effectively probed analytical depth will depend strongly on the particular analytical process used. Compared with other surface and near-surface analytical methods, IBA methods must generally be characterized as "surface-oriented" techniques, giving useful information from the first monolayers all through to tens of μm depth.

One serious issue of IBA is that the physical processes involved along the ion track will, in addition to producing useful radiation, also create modification and damage in the material. Such phenomena are utilized in the systematic ion beam modification and processing of materials, as described in Chap. 25. However, these processes could also pose a serious problem when a particular analytical application requires nondestructive analysis.

26.2 Experimental Facilities

There are many different types of IBA facilities, varying from those that are part of a large accelerator complex comprising almost all aspects of both basic and applied physics, to very small IBA labs around a small "turnkey"

accelerator, for instance specializing in specific routine analyses in large numbers.

Apart from a few cyclotron laboratories, two kinds of accelerators dominate IBA: single-ended and tandem electrostatic accelerators (see Chap. 4). The actual ion bombardment of specimens normally occurs in vacuum chambers fitted with an array of detectors suitable for different kinds of radiation. The complex multiparameter systems necessary for implementation of a number of detectors for different radiation components are often designed individually at each accelerator laboratory, while the computer codes used for evaluating spectral information and for simulation of ion–solid interactions are limited to a few well-established computer packages used at most laboratories [3, 4]. Lately, there have been attempts to build general-purpose software tools that will integrate several different analytical methods and the simulation of various compositions of materials. A review on how such a tool can be applied in elemental profiling of thin films is given in [5]. For special applications, for instance very near-surface studies, there may be requirements for sample heating/cooling, other types of specimen modifications, use of ultrahigh vacuum etc. Other specimens may be fragile and radiation-sensitive, requiring a minimization of heating and radiation dose. One approach that has been very successful in combination with valuable art objects is to extract the ion beam out from the vacuum system into air or other nonvacuum atmospheres [6, 7]. This type of analysis is particularly useful when analyzing large and sensitive objects and when investigating compounds of high vapor pressure.

A very important development within IBA is the use of highly collimated and focused ion beams for microscopic investigations. In fact, most of the traditional IBA methods are now applied also in such nuclear microprobes, where the high lateral resolution has resulted in completely new approaches to many analytical problems. The nuclear microprobe can be used to obtain quantitative analytical results from specific points on a specimen, but also for imaging a sample both qualitatively and quantitatively: the narrow ion beam is rapidly scanned over the specimen and, by measuring for a very short time in each pixel with sophisticated computer assistance, the results can, on-line or off-line, be related to the position on the specimen.

The greatest technical challenges in setting up a nuclear-microprobe system with a small beam focus originate from limitations in the present ion sources and technical difficulties in designing strongly focusing devices with low aberrations. One crucial parameter is the beam brightness B, a measure of the number of ions that pass through a given area with a given maximum divergence at a given energy. In a nuclear microprobe, brightness is defined as

$$B = \frac{i}{A_0(A_a/D^2)E_0} \tag{26.1}$$

where i is the beam current at energy E_0 that will pass through an object collimator of area A_0 and an aperture collimator of area A_a at a distance

D from the object collimator. The commonly adopted radio-frequency and duoplasmatron sources both suffer from relatively low brightness and are hence not ideal for nuclear microprobes. The development and adaptation to MeV beam optics of high-brightness sources such as liquid-metal or field-ionization sources have so far been of limited success [8].

A detailed investigation into the various types of focusing devices [9] is beyond the scope of this presentation but the clearly dominating type of device is the magnetic quadrupole in doublet, triplet or quadruplet configurations. A few laboratories use superconducting magnetic solenoids or electrostatic quadrupoles. In order to predict the smallest possible spot size on the specimen, one must consider the detailed action on the ions of the focusing elements and calculate the effects of the imperfect image formation. In addition to inherent components such as chromatic and spherical aberrations, parasitic aberrations originate from various errors in the design of optical elements. The most prominent factors are misalignment, power supply ripple and sextupole field components. Details of how to minimize these effects [10] are beyond the scope of this presentation. Each type of lens configuration has its virtues and drawbacks, and probe formation requires a tedious optimization process. In addition, stringent requirements on vacuum, electromagnetic stray fields, vibrations etc have to be fulfilled for minimum-size probe formation. In practical applications, most laboratories use a beam size $\geq 1\,\mu$m.

Based on lower-energy (200 keV) probes, commercially available high-resolution focused-ion-beam systems are already in use [11] that can perform RBS analysis (see Sect. 26.3) with better than 100 nm lateral resolution. Recently, in order to produce MeV ion beams with sizes <100 nm, work has started on the development of new high-demagnification systems in several laboratories [12, 13]. When the IBA methods are extended into such a very high-lateral-resolution mode, it is essential to develop suitable test structures. Such an attempt has been made by the Leipzig group [14], in a laboratory developing a nuclear "nanobeam" system. By growing a semiconductor heterostructure in GaInP on a substrate of GaAs, a sharp edge suitable for beam size calibration was obtained.

To make the most of such systems, the technical requirements on low vibrations etc. mentioned above, are even higher. In addition, the useful ion currents will be very low (tens of pA), which degrades counting statistics in the radiation detectors. Hence, several systems for very large-solid-angle detection are currently under development and implementation [15]. Figure 26.1 shows an eight-crystal X-ray detector (Canberra) that has a very large total solid angle with a maintained state-of-the-art energy resolution. The ion beam direction is shown by the arrow. Although such a detector system requires more complex data acquisition systems, it facilitates trace element determination using very low beam currents.

Also, in a nuclear microprobe it is possible to extract the focused ion beam into an atmosphere, albeit at the cost of degraded beam resolution because of

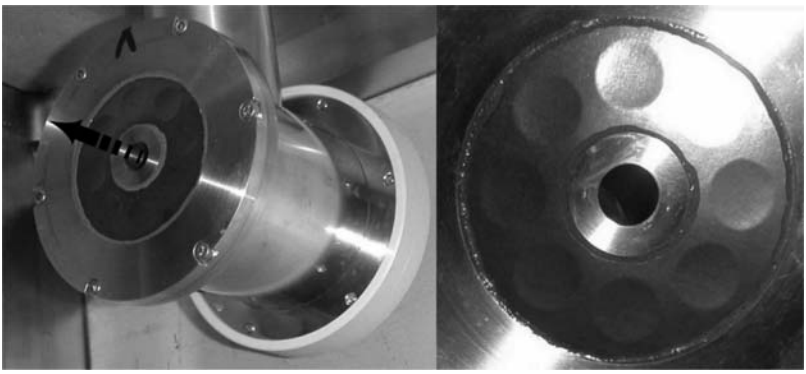

Fig. 26.1. Eight-crystal Ge X-ray detector (Canberra®) designed for enhanced X-ray detection efficiency in low-beam-current experiments [15]. The arrow indicates the ion beam direction. The resolution of each individual crystal is better than 150 eV at 5.9 keV

scattering in the exit foil and gas molecules. To reduce this degradation, the distance that the focused ion beam travels outside the vacuum is minimized by arranging very tight geometries between the detectors and the specimen.

26.3 Analytical Techniques

The great diversity of IBA methods makes it necessary to limit the following text to introducing a selection of existing techniques. The IBA techniques make use of a variety of physical interactions taking place after an ion impinges on the specimen surface. Since interactions can be both atomic and nuclear processes, the cross sections for the interactions vary by several orders of magnitude. As will be discussed in some detail later in this chapter, the technical amenities available will play a crucial role for each analytical procedure. The type of results produced varies from qualitative structural information, through semiquantitative elemental information on major constituents, quantitative trace elements and isotopic composition, to highly resolved depth profiling and lateral information. The nuclear microprobe described in Sect. 26.2 can normally integrate most of the existing IBA methods. The choice of IBA method will be determined by the specimens investigated and the specific information required. Owing to their reasonably nondestructive character, IBA techniques are, with great benefit, combined with complementary analytical methods.

26.3.1 Particle-Induced X-ray Emission (PIXE)

Ions of an energy greater than a few MeV/u impinging on a specimen have a high production cross section for inner-shell vacancies in the matrix atoms.

The subsequent deexcitation results either in a characteristic X-ray or in an Auger electron. Hence X-ray spectrometry can be performed for all elements heavier than sodium [16] (Auger electrons dominate over X-rays and attenuation is too high for lighter elements). Cross sections for inner-shell ionization are of importance when using PIXE. Several theoretical approaches have been used to calculate the cross sections, but the plane wave Born approximation model, which applies perturbation theory to a transition from an initial state to a final state, has been developed furthest, particularly by Brandt and coworkers [17, 18]. These authors incorporated a series of modifications into the initial model to correct for its inherent approximations, and this resulted in the so-called ECPSSR treatment of K and L shell ionization cross sections, which takes care of the deflection of the projectile due to the nuclear Coulomb field (C), perturbation of the atomic stationary states (PSS) by the projectile, relativistic effects (R), and energy loss (E) during the collision.

Calculation of the X-ray production cross section from the ionization cross sections involves additional atomic parameters: fluorescence yields and fractional radiative widths in the case of the K shell, and fluorescence yields, Coster–Kronig yields and fractional radiative widths for the L shell. As to the K fractional radiative widths, either the experimental data of Salem et al. [19] or the theoretical values of Scofield [20] are used. For the case of the L X-rays Campbell [21] advocates the use of the radiative widths of Scofield [22] and the fluorescence and Coster–Kronig yields of Chen et al. [23] in combination with the tabulated L ionization cross sections of Chen and Crasemann [24].

A practical alternative to tabulated theoretical ionization and X-ray production cross sections, particularly with computer calculations in mind, is analytical formulas which are obtained by fitting polynomial expressions to theoretical or empirical cross-sectional data [25, 26]. For the proton energy range of 1–4 MeV typically used in PIXE, the ionization (and X-ray production) cross sections increase with increasing proton energy and decrease with increasing atomic number of the target atom (see Fig. 26.2).

Continuous-Photon-Background Production

The characteristic X-ray lines in a PIXE spectrum are superimposed on a continuous background (see Fig. 26.3). The interactions of charged particles and matter occur mainly through inelastic encounters with bound electrons. This results in electron excitation and ionization but also in secondary phenomena that contribute to the background, which is very important since the peak-to-background ratio for each characteristic X-ray line will determine the detection limits for the PIXE method.

Electron Bremsstrahlung

Electron bremsstrahlung is the major background component. In the mid 1970s, Folkmann et al. [27] and various coworkers made very significant

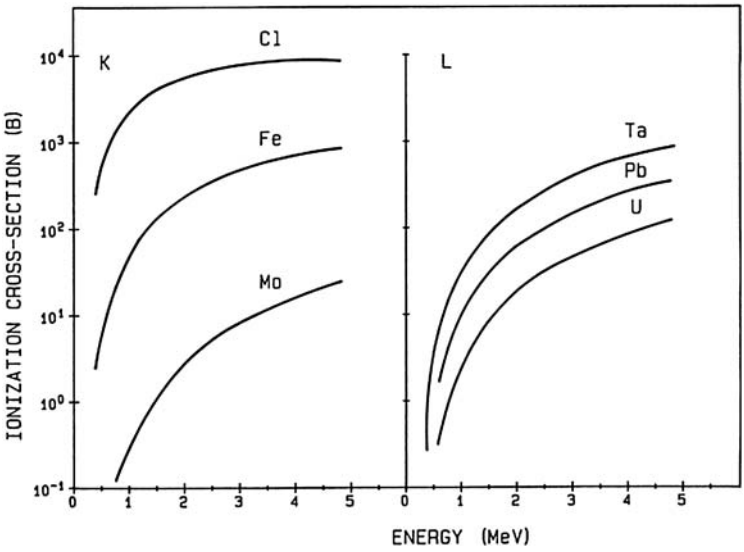

Fig. 26.2. K and L ionization cross sections vs. proton energy for several elements

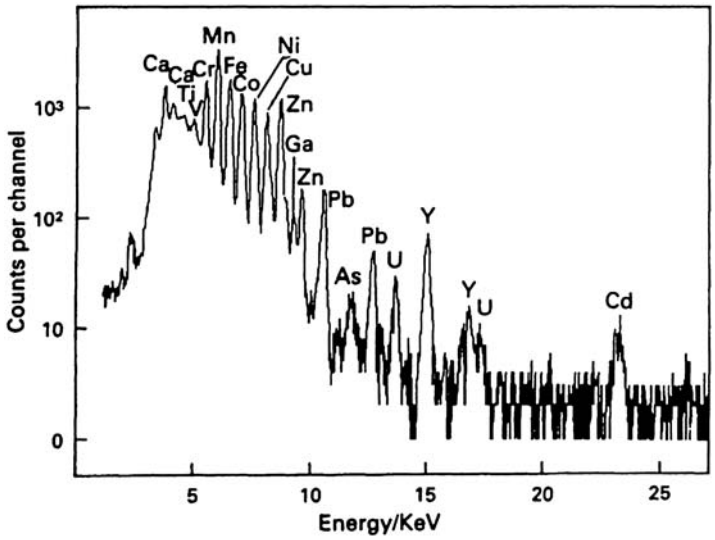

Fig. 26.3. Typical PIXE spectrum, showing several characteristic X-ray lines superimposed on a continuous background

contributions to our understanding of the continuum background in PIXE, which were later complemented and extended by Ishii and Morita [28]. Electron bremsstrahlung in PIXE originates essentially from three processes: quasi-free-electron bremsstrahlung, secondary-electron bremsstrahlung and atomic bremsstrahlung. Besides the energy of the impinging ion, the matrix composition of the target plays a critical role in both the shape and the intensity of the electron bremsstrahlung background. The intensity of this background per unit mass thickness is roughly proportional to the average Z of the matrix. The electron bremsstrahlung is emitted anisotropically and is lower at forward and backward angles than at 90°. For this reason, the X-ray detector is frequently positioned at an angle of 135° relative to the ion beam.

Projectile Bremsstrahlung

While passing through the target, the incident charged particles may be decelerated in the Coulomb field of atomic nuclei and thereby give rise to the emission of projectile bremsstrahlung [27]. Although this process is negligible within the context of the projectile energy loss, it contributes to some extent to the continuum background in the PIXE spectra. It is much less important than the electron bremsstrahlung and only becomes significant at photon energies above 10–20 keV.

Experimental Details

In a typical setup for broad-beam PIXE analysis, several samples are simultaneously inserted into the vacuum, to facilitate a high sample throughput. PIXE spectra have most of their characteristic and continuous X-ray intensity in the low-energy region, so that the spectral shape can advantageously be modulated by placing an X-ray absorber between the sample and the detector. The aim of an absorber is to reduce or eliminate unwanted continuum background and/or intense X-ray peaks and their associated pileup peaks and at the same time to allow bombardment at higher beam intensities, so that the elements of interest can be measured in shorter bombardment times and with fewer spectral interferences. In many cases it is preferable to allow a certain fraction of the low-energy X-rays to pass on onto the detector. This can elegantly be realized by resorting to pinhole absorbers. Also, more sophisticated designs consisting of a combination of various layers with different thicknesses and pinhole diameters have been used [29].

The energy-dispersive detectors used for PIXE are the same as those in other X-ray spectrometry techniques. They typically have a sensitive area from 10 to 80 mm^2. In ion beam analysis systems based on nuclear microprobes, the ion current for very narrow beams may be very low (tens of pA), and hence new multicrystal detectors are being developed [15] (Fig. 26.1). The ion beam passes through the center of the detector (see arrow) and

the crystals are oriented annularly, facing the specimen surface. The amplifiers/pulse processors in energy-dispersive X-ray spectroscopy require large time constants for optimum energy resolution. Unfortunately, large time constants also imply that pulse pileup becomes a serious problem at relatively low count rates. It is therefore common practice to incorporate an electronic pileup rejector and its associated dead-time correction circuitry in the pulse-processing chain.

The bombardment of an insulating thick (or semithick) specimen in vacuum generally gives rise to charge buildup, and the specimen may reach a positive potential of up to several tens of kV before breakdown and sparking. The high potential accelerates electrons to up to tens of keV, and as a consequence an intense bremsstrahlung background is produced in the PIXE spectrum. The peak-to-background ratios then decrease significantly [30].

Quantitation and Sensitivity

The basis for a quantitative analysis is that there is a relationship between the net area of an element's characteristic K or L X-ray line in the PIXE spectrum and the amount of element present in the sample. For proton bombardment and an infinitely thin specimen (by this is meant a specimen that is sufficiently thin that matrix effects become negligible), the relation is given by

$$Y_p(Z) = \frac{N_0 \sigma_{pZ}^X(E_0) \epsilon_p N C_Z \rho t}{A_Z \sin\theta} \tag{26.2}$$

where $Y_p(Z)$ is the number of counts in a characteristic X-ray line p of the element with atomic number Z, N_0 is Avogadro's number, $\sigma_{pZ}^X(E_0)$ is the X-ray production cross section for line p at the incident proton energy E_0, ϵ_p is the absolute detection efficiency (including the solid angle) for X-ray line p, N is the number of incident protons, C_Z is the concentration of the particular element in the specimen, ρ is the specimen density, t is the specimen thickness, A_Z is the atomic mass of the element, and θ is the angle between the incident proton beam and the specimen surface. In formulating this equation, it is implicitly assumed that the specimen is uniform and that the beam size is smaller than the specimen area.

In practice, specimens are rarely thin enough for matrix effects to be entirely negligible. For specimens of intermediate thickness and for infinitely thick specimens (the latter are specimens that are thicker than the particle range), the quantitation equation has to include a correction for projectile slowing down and X-ray attenuation.

The minimum detection limits for PIXE depend both on matrix composition and on the element under investigation. By using both K and L X-rays, a good sensitivity across the periodic table is obtained. In routine analysis, the detection limits are of the order of 0.1–1 μg/g. With optimization of the experimental parameters, an improvement by a factor of 10 can be achieved.

26.3.2 Backscattering Spectrometry

The acronym RBS (Rutherford backscattering spectrometry) is often used for a variety of techniques based on detection of ions scattered by target nuclei [31]. The energy of the scattered projectile is measured and related to the mass of the scattering nucleus (see Fig. 26.4), as well as to its position in the matrix. The characteristics of RBS make it particularly useful for determination of depth distributions of heavier elements in light-element matrices and for investigation of thin multilayer films. For purely elastic collisions, the incoming ion will not have sufficient energy to penetrate the Coulomb barrier, and classical mechanics can be applied. In this Rutherford energy regime, the energy of the scattered ion and the probability for scattering are described by the Rutherford equations:

$$E = \epsilon_0 \frac{m_1^2}{(m_1 + m_2)^2} \left[\cos\theta + \left(\frac{m_2^2}{m_1^2} - \sin^2\theta \right)^{0.5} \right]^2 \tag{26.3}$$

$$\frac{d\sigma}{d\Omega} = 1.296 \left(\frac{zZ}{E_0} \right)^2 \left[\sin^{-4}\left(\frac{\theta}{2} \right) - 2\left(\frac{m_1}{m_2} \right) + \ldots \right] \tag{26.4}$$

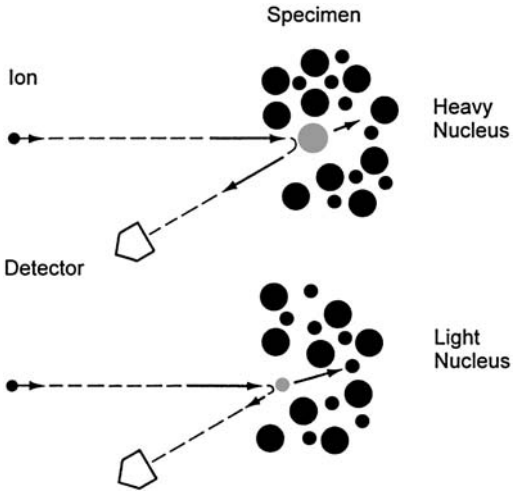

Fig. 26.4. The basic principles of ion backscattering spectrometry

Here m_1 and m_2 are the masses of the incident ion and target nucleus, E_0 is the energy of the ion scattered at a given depth, and z and Z are the charges of the ion and of the scattering nucleus, respectively. By measuring the energy of the scattered ions at a well-defined angle θ, the mass of the scattering nuclei can be determined. As is discussed in Chap. 24, the energy

loss of an ion traversing a relatively well-known matrix can be accurately calculated, as well as the energy loss of the scattered ion on its way through the matrix to the detector. Hence, this method can produce quantitative depth profiling of the isotope studied. Since a realistic analytical situation is much more complex than one single element in a fairly well-characterized matrix, practical analytical procedures require computer-based simulations based on any previous knowledge of the material studied.

In classical RBS, the ions are normally selected to be 2 MeV α-particles. This allows simultaneous PIXE analysis and fulfils the Rutherford requirements. To increase sensitivity and depth resolution, it is possible to use much heavier ions [32] and combine this approach with a time-of-flight detection system [33]. When heavier ions are used, beam-induced damage increases and has to be taken into account. When RBS is combined with PIXE for simultaneous X-ray spectrometry, the ions are normally protons of 2–5 MeV and then the classical Rutherford conditions are not fulfilled. Since protons partially penetrate the Coulomb barrier, they can produce resonant scattering and nuclear reactions that will generate much more complex scattering spectra. Although the interpretation of these spectra will hence be less straightforward, such resonances can also be used to enhance sensitivity for selected isotopes, and the quantitation and interpretation can be assisted by using suitable reference materials.

Experimental Details

The angle at which the scattered ions are detected will determine the characteristics of the RBS measurements. The mass resolution is highest at an angle of 180° relative to the incoming ion beam, and hence the detectors used to measure the ion energy are often placed at a large angle in the backward direction, for instance in the form of an annular detector facing the specimen with the incident ion beam going through a central hole. The resolution is limited by several factors: energy straggling of the scattered ion in the matrix and the intrinsic energy resolution of the detector used. Detecting at approximately 90° increases the scattering cross section, energy straggling and depth resolution, while the mass resolution will be poor. Normally a semiconductor detector is used, but for very high demands on resolution either a time-of-flight (ToF) system or a magnetic spectrometer [34,35] can be used.

The applications of RBS that dominate by far are within materials science and to study thin layers and depth distributions. Normally good previous information is available on each specimen, which makes it suitable to simulate expected RBS spectra and to compare the simulations with experimental results. Several computer codes are available [3, 36]. For absolute calibration various reference materials are commercially available. In addition, materials science studies often require that experiments are performed in ultrahigh

vacuum and that the specimens can be manipulated during analysis, for instance by heating, cooling or sputtering. Furthermore, since analysis is often performed on single crystals, the specimen needs to be mounted on a multiaxis goniometer. As is discussed in Chap. 24, the ion penetration depth will increase when an incoming ion channels along a crystal axis. Hence, the probability of close encounters such as ion/nucleus scattering is also reduced, and the RBS yield from lattice atoms, as well as substitutional atoms, will be much reduced (by approximately an order of magnitude) along the crystal axis. The yields from other types of close-encounter interaction, for instance PIXE, will also be reduced. By varying the orientation of a crystal mounted on a goniometer and registering RBS signals, the crystalline structure, including potential dislocations and possible interstitial atoms, can be investigated [37]. The quality of crystal lattices, epitaxial layers and lattice strain can be investigated by such ion channeling.

Another type of MeV ion-scattering spectrometry, particle elastic-scattering analysis (PESA), is best applied to thin targets, i.e. targets fully penetrated by the incoming ion. By registering ions scattered into forward angles a high flux (high scattering cross section) is available, but since the mass separation in forward angles is low, this technique only lends itself to measuring low-Z elements. Since several low-Z elements are of interest in many analytical applications and these elements are difficult to measure by other means, the main use of PESA has been as a complementary technique to, for instance, PIXE.

26.3.3 Elastic-Recoil Detection Analysis (ERDA)

Instead of measuring the scattered ions, ERDA [39] exploits the target atom recoil in the forward direction in a glancing-angle geometry. For thin specimens, transmission ERDA is also possible [40]. Recoiling atoms lighter than the incoming ion will receive a higher energy than the corresponding scattered ions, which will hence be easy to eliminate with stopping foils. Hence, ERDA is ideal for profiling light isotopes in a matrix with an abundance of heavier elements. Owing to low cross sections for forward recoiling, the analytical sensitivity is not very high, but the depth distribution of the order of a few nm. A typical analytical situation, shown in Fig. 26.5, would be to use an alpha particle beam of a few MeV to investigate a hydrogen diffusion profile.

One limitation in the traditional experimental ERDA setups is the energy resolution of the semiconductor detector. ToF systems in conjunction with recoil spectrometry comprise an energy detector and two thin foils used as start and stop detectors, making use of secondary electrons produced in each foil. The measured flight times are then plotted vs. recoil energy. This type of recoil spectrometry can also be applied with high-energy nuclear microprobes although the ion currents are significantly lower than in normal IBA facilities.

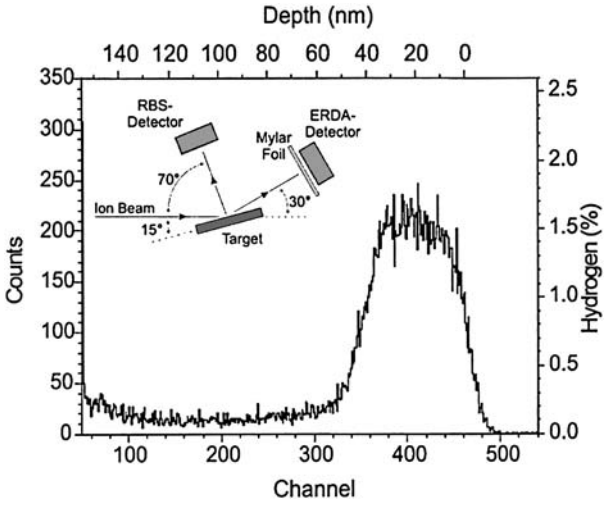

Fig. 26.5. Typical ERDA setup with an additional RBS detector, and an ERDA spectrum showing a hydrogen depth profile based on an alpha particle beam (Reprinted from [38], copyright 2002, with permission from Elsevier)

This requires a detector system with a large solid angle to compensate for the low cross sections for recoils in the forward direction [41].

For experimental facilities with high-energy accelerators and heavier ions, other recoil techniques can be used. Using high-energy-resolution detection, it is then possible to simultaneously profile light to medium-heavy elements in matrices of lighter and/or heavier elements [42].

26.3.4 Nuclear-Reaction Analysis (NRA)

The cross section for a nuclear reaction depends in a complicated manner on the incident ion energy and the internal properties of the particles involved. The Coulomb barrier is approximately

$$E = \frac{zZ}{(a^{1/3} + A^{1/3})} \text{ MeV} \tag{26.5}$$

for an incident ion of atomic number z and mass a and a target nucleus of mass A and atomic number Z. The projectile will normally not interact strongly in a nuclear reaction unless the incident energy is greater than the Coulomb barrier. Clearly, for moderate ion energies, nuclear reactions will only occur with the lightest target element. Hence, a light ion of MeV energy can overcome the nuclear charge of low-Z matrix elements, and inelastic reactions can occur. The existence of particular nuclear reactions with relatively high cross sections represents a potential for accurate trace element determination of specific light isotopes in high-Z matrices [43].

The nuclear reaction occurring is either a direct reaction or a compound-nucleus reaction. In the latter case, an intermediate-state excited nucleus forms that will eventually decay by gamma rays or charged-particle emission. By detecting these radiation quanta, analysis of light elements can be performed. A common example of this type of NRA is the use of ^{19}F(p, $\alpha\gamma$)^{16}O for depth profiling, thereby making use of sharp resonances in the cross section as a function of proton energy [44]. In contrast to compound formation, the direct-mechanism nuclear reactions normally demonstrate a cross section smoothly varying with energy, for instance in the case of ^{13}C(d, p)^{14}C [45]. There are many combinations of ions and elements that facilitate analysis by specific nuclear reactions. The possibility of measuring lighter elements, such as boron, beryllium and nitrogen, is a major advantage in combination with techniques such as RBS and PIXE, which are more suited for measuring medium-heavy and heavy elements.

The special case of particle-induced prompt gamma rays is often denoted by the term particle-induced gamma-ray emission (PIGE) [46]. It has been used extensively in simultaneous combination with PIXE and is normally defined as detection of prompt gamma rays produced during MeV ion bombardment of a specimen homogeneous in depth, i.e. resonant reactions are not used for depth profiling. Because of the interaction occurring with the nucleus, the cross sections are lower than for PIXE, and PIGE typically represents a less sensitive analytical technique than PIXE. However, the gamma-ray peaks are generally well isolated and the energy of the emitted gamma-ray photons is high enough that correction for attenuation will not be necessary. PIGE may hence in some situations be favorable compared with PIXE for elements such as calcium and potassium [47].

The high penetration of gamma rays also simplifies the experimental arrangements, and the nuclear interaction facilitates the obtaining of isotopic information. External beams are a standard method in the case of PIGE [48] and offer the same advantages as discussed above for the case of PIXE.

In Tables 26.1 and 26.2, some examples of the detection limits of PIGE are given. They are given only as indications of attainable sensitivities, since the specific experimental conditions will have a strong impact. The values in these tables apply when the experimental arrangements and bombarding energy are optimized for the detection of a specific element.

Table 26.1. Detection limits (atomic fraction) for PIGE using protons ($E_p <$ 9 MeV) [49]

>1%	0.1–1%	<0.1%
Pd, Sm, Gd, Hf, W, Au, Pb	S, K, Sc, Ti, Co, Cu, Ge, Y, Zr, Mo, Ru, Ag, Sn, I, Ta, Pt	Li, Be, B, C, N, Na, Mg Al, Si, Cl, Ca, V, Mn, Fe, Ni, Zn, Nb, Cd, In, Sb

Table 26.2. Detection limits (atomic fraction) for PIGE using α-particles (5 MeV) [50]

>1%	0.1–1%	<0.1%
Sc, Cr, Cu, Zn, Rb Zr, Er, Hf, Hg	O, Mg, Si, Cl, K, Ti Fe, Br, Mo, Ru, Pd Ag, Cd, Ta, W, Re Ir, Pt, Au	Li, B, N, F, Na, Al, P V, Mn, Rh

26.3.5 Scanning Transmission Microscopy (STIM)

When using a nuclear microprobe to investigate nonhomogeneous, thin (ions will pass through) specimens, it is very useful to measure the actual "mass" thickness (mg/cm^2) in each analyzed "pixel". The well-defined energy loss of ions facilitates calculation of this thickness from the energy loss through the specimen. One can use direct or indirect determination of the energy loss for each individual ion when it passes through a thin specimen [51]. The drawback of STIM in direct mode is that it is a stand-alone technique and cannot be combined with, for example, simultaneous PIXE or RBS measurements, because the ion beam intensity has to be extremely low (1000–10 000 ions/s) not to saturate the detector. With a traditional off-axis geometry, STIM can be performed in parallel to both PIXE and RBS because the beam current is typically 50 pA or more. A drawback with off-axis geometry is that it has an inherent spectral degradation. An alternative geometry, called on-axis/off-axis STIM, combines the advantages of both on-axis and off-axis STIM. This geometry is sensitive only to pure energy loss in the sample. No ions scattered in the sample will influence the spectral shape, because those ion paths are collimated off. Instead, a part of the transmitted beam is scattered into the detector by a thin monoelemental foil situated behind the sample. By varying the scattering angle from the foil, the count rate of the STIM detector can be matched to the actual beam current used, and thus STIM measurements can be done in parallel with, for example, PIXE measurements. STIM offers structural imaging of specimens but also facilitates normalization of the results of other analytical methods to the mass in each analyzed pixel.

Sub-cellular mass determination in organic material or tissues using STIM is crucial for accurate normalization of concentrations by PIXE. A good illustration of what can be obtained by STIM is an investigation where 2 MeV α-particles were used to map an intracellular mass distribution [52]. Freeze-dried cells were investigated and compared with results from cellular sections in epoxy resin, and this facilitated accurate quantitation of the intracellular elemental concentrations. Another example of STIM images from freeze-dried tissue is shown in Fig. 26.6, clearly demonstrating the cellular structure.

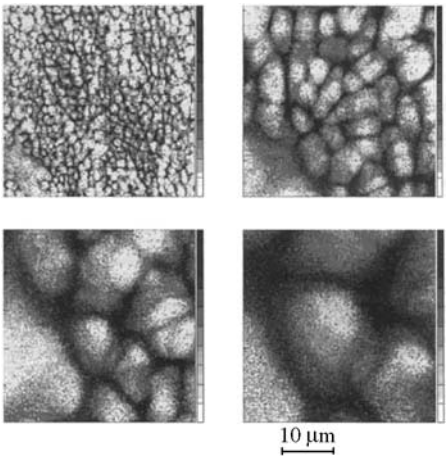

Fig. 26.6. STIM images from a section of freeze-dried brain tissue at different magnifications. The individual cells are easily observed (Courtesy of P. Kristiansson)

Although the focused microbeam does not yield an ideally parallel beam for channeling, the STIM technique can be applied also in channeling mode for crystalline structures. Along the crystal axes, the ion penetration depth will be much increased and less energy will be lost. By rastering the microbeam over the specimen, it is possible to check the lateral variation in the ion channeling intensity due to the existence of regions with imperfect crystalline structure. This method is called channeling contrast microscopy [53] and is useful in materials science applications.

In another development, STIM can be used for tomographic reconstruction [54] of microscopic objects. By rotating and translating a specimen through a narrow ion beam and measuring the energy loss, a computer code can be used for subsequently reconstructing the inner structure of the specimen. When STIM is combined with X-ray detection, PIXE can facilitate reconstruction of 3-dimensional elemental distributions [55]. In Fig. 26.7, ion-tomographic reconstructions of the mass density and manganese content in a scorpion stinger are shown across the stinger. The stinger is very brittle and would break during sectioning, making a noninvasive technique necessary.

26.3.6 Ionoluminescence (IL)

The same mechanisms that create characteristic X-rays, as discussed in Sect. 26.3.1, also produce intense visible or UV light from the outer shells during ion bombardment. In transparent matrices this can be utilized for imaging and analytical purposes, similarly to cathodoluminescence as used in an electron probe [56]. The physical processes creating luminescence are similar for electrons and ions, but since the electron and ion beams have quite different

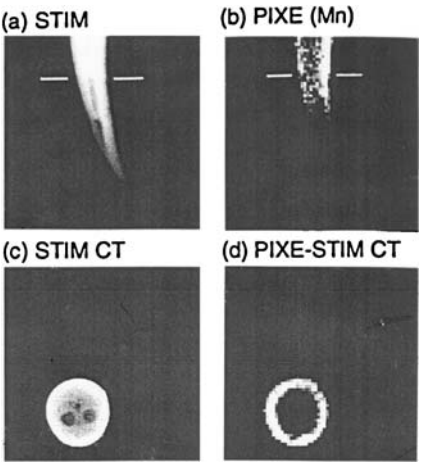

Fig. 26.7. Characterization of a scorpion stinger by a nuclear microprobe: (**a**) STIM image, (**b**) PIXE elemental map of manganese, (**c**) computer-reconstructed mass distribution at the level in the stinger given by the white lines in (a) and (b), (**d**) computer-reconstructed manganese distribution at the same level. The analysis clearly shows high levels of manganese at the stinger surface as a result of the biomineralization process (Courtesy of R.M.S. Schofield)

matrix penetration characteristics, they are complementary to each other. Luminescence phenomena are common in many solids, yet the use of the light produced is restricted because of the complex physical mechanisms behind the emission. For insulators, to which many minerals belong, crystal field theory can be used to explain luminescence, whereas for semiconductor crystals, band theory is often employed. Luminescence can be divided into two subgroups, intrinsic and extrinsic, according to its origin. In a material with a band gap between the conduction band and valence band, the extrinsic luminescence depends on donor and acceptor levels that are related to impurity ions. The intrinsic luminescence usually contributes to emission through crystal structural defects and hence to crystal lattice properties. Ionoluminescence [57] depends on the characteristics of the specific luminescence centers in the material.

Although IL can yield information on both crystal structure and the chemical state of the atoms present, it is in practice so far limited to semiquantitative analysis. In geochemistry, rare-earth elements (REEs) are often very important and, owing to specific characteristics of the electron configuration for all trivalent and several divalent REE ions, IL represents a particularly good complement to PIXE, which has a particularly low sensitivity for these elements [58]. The narrow luminescence emission bands of the REE ions are caused by electrons in the 4f subshell, which is partially shielded by ($5s^2 5p^6$) electrons. Since the interaction between the 4f electrons and the crystal field

is weaker than the spin–orbit interaction and the energy levels of REE ions of this configuration are not significantly influenced by crystal fields, the structure of the energy levels in the free REE ions is basically the same in different host matrices.

Experimental Considerations

A nuclear microprobe is normally operated in combination with IL in two ways, spot or scanning mode. Furthermore, the light produced can be analyzed in a spectrometer system with a grating monochromator in combination with a photomultiplier tube (PMT) or directly into the PMT (panchromatic mode). In Fig. 26.8, three elemental maps from PIXE are compared with a photographic image and a panchromatic IL map. Another possibility is to scan the specimen and record the image produced in a very sensitive CCD camera. Using a grating monochromator, high-resolution IL spectra can be acquired in spot mode and be combined with simultaneous PIXE analysis for trace element determination.

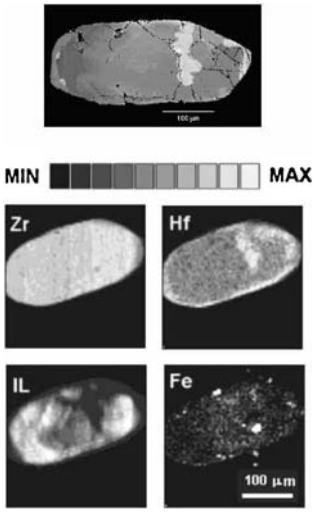

Fig. 26.8. Panchromatic IL image and three PIXE elemental maps from a natural zircon

High-resolution spectra normally require long times of irradiation (minutes), which also means high radiation doses and thus a change in the IL emission during irradiation. By employing a photodiode-array detector with many elements, a few tens of µm each, a rapid high-resolution system can be obtained. It allows the simultaneous recording of all wavelengths, significantly improves the analytical capacity and reduces beam damage effects [59].

26.4 Applications

In the following, a selection of applications is presented in order to illustrate the various characteristics of IBA methods. The selection is also intended to demonstrate typical fields where IBA has had a major impact, although many times in conjunction with other analytical techniques. In fact, the most successful studies involving IBA methods also make use of an arsenal of analytical tools to complement the special characteristics of IBA methods.

In order to illustrate the present status of IBA applications, the latest International Conference on Ion Beam Analysis (IBA 2003, Albuquerque [60]) may offer a deeper insight. As in earlier conferences in this biannual conference series, the contributions are still dominated by traditionally common applications such as thin-film analysis by RBS and ERDA, trace element analysis by PIXE, and light-element analysis by NRA. Altogether these applications represent approximately 2/3 of the contributions submitted and are mainly related to materials analysis. However, novel methods and new developments, for example, nanoscience [61,62], within existing fields are becoming of growing importance. In other conference series, many other fields of application, such as the environment biomedicine and archaeology, are addressed.

26.4.1 Materials Science and Industrial Applications

In a broader sense this field covers such varying areas as electronic devices, metallurgy, geology, the arts and archaeology. However, normally one would limit this field to refer only to the study of technological developments of modern materials.

In the early days of IBA, RBS soon became one of the standard techniques for surface characterization of semiconductors and was also adopted in industrial processing environments. Since the detailed crystalline structure and possible defects were often of great importance, RBS was also combined with crystal channeling phenomena. With the subsequent development of the various analytical techniques in IBA, these techniques were often integrated in various simultaneous combinations (e.g. RBS, PIXE and NRA) for materials characterization. One very good example of this is the characterization of magnetic thin films using a spectrum of various IBA methods. Both α-particles and deuterons are used as bombarding ions, and by combining several methods detailed information has been yielded [63]. In the semiconductor industry today, in-house accelerators are used in R&D and for process quality control. In order to extend the industrial IBA arsenal, NRA based on deuterons is used as a complement to RBS for lighter-element characterization [64].

With the growth during the last decade of complex materials in parallel with a very strong trend toward nanoscience and nanotechnology, IBA techniques have developed accordingly. One such example is an investigation of

quantum well structures in SiGe by using high-resolution channeling contrast microscopy [65]. Using RBS in channeling mode and the high lateral resolution of the nuclear microprobe, it was possible to identify microscopic lateral inhomogeneities associated with a slight lattice tilt present in the specimens studied. Another example of the use of this technique is an investigation of ion-etched silicon microstructures [66]. In Fig. 26.9, images from scanning-electron secondary electrons and channeling-contrast microscopy can be compared.

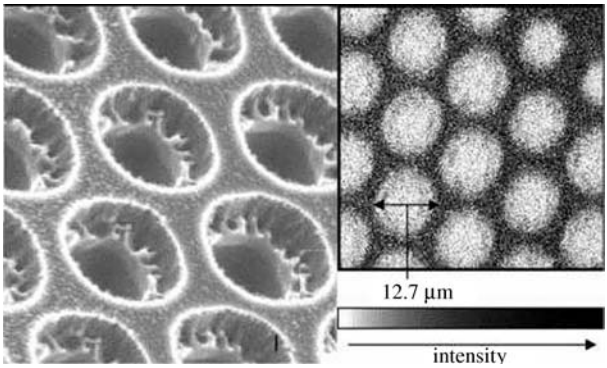

Fig. 26.9. Silicon microstructure imaged by electron secondary electrons and channeling-contrast microscopy (Reprinted from [66], copyright 2002, with permission from Elsevier)

Depth profiling of hydrogen is a common and technologically very important application of IBA. Several methods can be applied, for instance ERDA with He ions and NRA using ^{15}N ions. Samlenski et al. [38] used 2.8 MeV He^+ ions for high-lateral-resolution ERDA measurements on CVD-grown diamond and could relate the hydrogen maxima found to to observed optical structures (see Fig. 26.5). They also complemented these measurements with ^{15}N profiling. This is one example of a very common analytical problem in surface and thin-films analysis where IBA methods have made significant contributions owing to their high depth resolution characteristics. Recently, the theoretical and experimental limitations on depth profiling due to multiple scattering phenomena have been investigated in detail [67].

Another important materials analysis aspect is the use of IBA to monitor the results of another means of using ions in solids, ion implantation. After controlled ion-beam-assisted materials modification, which is regularly used in the production of semiconductor devices (Chap. 25), it is very suitable to use different IBA methods to control the effects of the irradiation. In fact, it is possible to perform this investigation on-line, i.e. to measure during ion beam processing. A Japanese group did this when implanting deuterons by monitoring the yield from the ^{2}H(d, p)^{3}H reaction [68]. The emitted protons

were counted as a measure of the deuteron fusion intensity. The group were able to show large differences in proton emission intensity between single-crystal and polycrystal areas in tantalum but not in copper matrices.

The industrial applications of IBA were initially limited to materials characterization using primarily RBS, but recently new approaches have been investigated. Wood-based industries are a very economically important industrial field in both Sweden and Finland, which probably has initiated a rather extensive collaboration with this normally rather "low-tech" base industry. In Sweden, in a direct collaboration with the paper industry, PIXE and STIM in a nuclear microprobe were used for studying the details of printing on newsprint paper [69]. The STIM measurements assisted in showing the mass distribution of the fibrous structure, as demonstrated in Fig. 26.10. By combining STIM with PIXE measurements, it is possible to investigate how the ink from printing is distributed in the fibrous structure and to understand how the smearing of the ink on newsprint paper can be reduced [70].

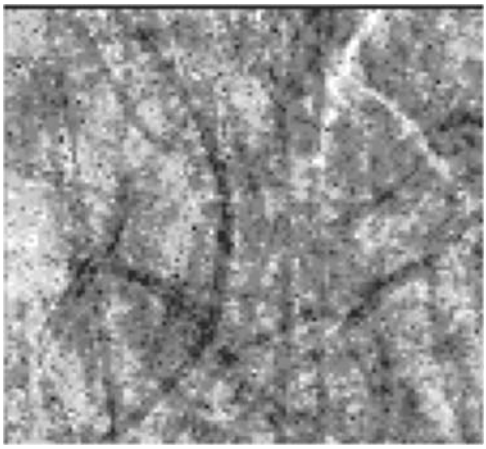

Fig. 26.10. STIM image of newsprint paper revealing the fibrous structure (courtesy of P. Kristiansson)

In a Finnish study, wood material delivered to pulp industries was pre-analyzed by PIXE in order to know the trace element concentrations to minimize discharge of polluting effluents [71] from the processing of pulp.

Another example of innovative "industrial" use of IBA techniques is the study of "hot" radioactive material, as carried out at a dedicated beam line at the Pierre Suë laboratory, Saclay, France [72]. By directing the ion beam into a hot-cell beam line, nuclear-microprobe experiments can be carried out by remote control. IBA methods have also been used to monitor actinide concentrations in drainage from a radioisotope laboratory [73]. By the combined use of a preconcentration technique and PIXE analysis, thorium and

uranium could be analyzed quantitatively down to 5 ppb in the drainage. Another interesting example in the same field is the investigation of actinide transport in granite microstructures in bentonite clay a material favored by many experts as an ideal barrier when storing radioactive waste [74]. The combined use of PIXE and RBS was used to investigate diffusion processes.

26.4.2 Geosciences

The geosciences have traditionally been a very strong field of IBA application, since the beam-induced radiation damage in mineral samples is normally negligible. There are several IBA laboratories that have had a strong focus on geosciences or even have been entirely dedicated to the field and worked both in basic research and in applied ore prospecting. The nuclear microprobe, with its inherent high lateral resolution, is particularly suitable for investigating the microscopic structure of minerals. The CSIRO laboratory in Sydney* [75] has been commendable for a very user-oriented activity that approaches both basic problems and industrial partners. It has also recently upgraded its nuclear microprobe to be even better prepared to approach specifically mineralogical problems [76].

An example of a typical application is a study of trace elements in sulfides to provide insights into various geological processes such as ore formation and magmatic-system evolution [77]. By combining traditional electron microprobe and ion-sputtering mass spectrometry probes with PIXE analysis in a nuclear microprobe, several trace constituents of the sulfides could be accurately quantified and used for understanding, for instance, ore formation processes. In another study of sulfides [78], PIXE results were compared with laser ablation microprobe–ICP measurements and could confirm that the laser ablation analysis gave reasonably accurate quantitative results.

Owing to a lack of suitable methods, it is very difficult to localize and quantitatively analyze boron in minerals. By developing an NRA method based on the reaction ^{11}B(p, α)2α, which has an especially high cross section for 660 keV protons, it was possible to analyze B at low concentrations in calibrated single crystals [79]. This method has later been applied successfully to real geological specimens. Also, PIGE can be successfully applied in geological applications. The combined use of PIXE and PIGE in investigations of fluid inclusions in minerals is a powerful technique, and PIGE contributes with concentrations of light elements, such as Li, Be, B and Na [80]. Using this analytical combination, many disadvantages of the traditionally used destructive methods, for instance laser ablation–ICP, can be avoided, and a good analytical accuracy is obtained.

Also, applications that do not make use of a microbeam but rely only on the high sensitivity of the PIXE method can contribute significantly in prospecting for ores. The geogas technique [81] is based on the principle of

* This lab has just recently (2004) been relocated to Melbourne univ.

tracing the weak signatures of deep mineralizations on the surface of the ground. In geogas prospecting, extremely small concentrations of trace elements, in an upward gas stream collected on thin membranes, are measured using the PIXE technique. The elemental composition of the geogas across geological formations reveals much about the bedrock composition and the possible presence of concealed mineralizations and ore bodies.

26.4.3 Biology and Medicine

Although organic materials are rather sensitive to ion-beam-induced damage, ion beam techniques, in particular PIXE, have had and still have a significant impact on biology and medicine for localized trace element analysis. With the development of the nuclear microprobe, bioscience obtained a versatile tool to add to the existing methods of microanalysis. It is being used for a wide spectrum of biomedical applications, varying from investigations of human kidney stones [82], through the elemental composition of beetles [83], to single marine toxin-producing phytoplanktons [84].

A recent example of how the technique can be applied at single-cell level is a study of clinical oncology using gallium nitrate for antitumor action. Since the reasons for this action are not fully known, ovarian cancer cells were exposed to gallium nitrate and analyzed by a nuclear microprobe [85]. In most cells the gallium was distributed homogeneously in the cells, but in some cells it was concentrated in a well-localized, perinuclear region. This finding contributed considerably to new information on how gallium attacks tumor cells.

Another anticancer treatment relies on specific localization of a boron compound, BPA, in cancer cells, and subsequent neutron exposure and boron neutron capture therapy. The tumor-to-tissue ratio of the boron concentration, as well as the location of boron within the cells – the α-particles produced in the $^{10}\mathrm{B(n, }\alpha)^{7}\mathrm{Li}$ reaction only have a range of about 10 µm (a cell diameter) – is critical for the efficiency of this therapy. Using the same reaction for boron detection as described in Sect. 26.4.2, a nuclear microprobe was used to investigate the intracellular boron concentration and distribution [86]. Alpha particles were detected in the forward and backward direction simultaneously. Only the coincidences between the two directions were then considered to be true boron events, resulting in excellent background suppression. The boron abundance was found to be 150 ± 20 ng/cm^2 in normal tissue and 570 ± 70 ng/cm^2 in tumor tissue. However, if the rats were fed with L-dopa prior to the injection of the boron-carrying drug BPA, the uptake in cancer tissue increased 3 to 4 times. Furthermore, the boron seemed to be homogenously distributed in the cellular structure and no specific accumulation close to the nucleus was shown (see Fig. 26.11, where boron events are marked as black dots and overlaid on the STIM image).

Nuclear-microprobe analysis of plants has had significant implications in plant science in general, but in particular in the understanding of species

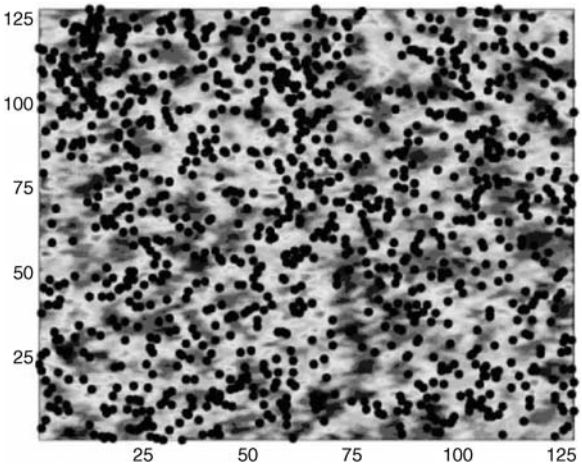

Fig. 26.11. Boron distribution (*black dots*) as measured by a nuclear microprobe in a tumor tissue from a rat brain, superimposed on a STIM map [86]. The rat was infused with the boron-carrying drug BPA after being pretreated with L-dopa

demonstrating hyperaccumulation of metals [87]. The importance of adequate sample preparation was shown in a study of a Ni-hyperaccumulating plant. It was demonstrated that new and more sophisticated techniques of freeze-substitution techniques are required for accurate ultrastructure measurements with a nuclear microprobe [88].

The nuclear microprobe has been very useful in the field of limnology and marine sciences for the investigation of mineralized tissue such as shells or bones. The fixation of various elements during growth generates a time chart of elements that may be utilized for the understanding of changes in the environment surrounding the organism in question. One such specific structure that is being used extensively is the otolith, a biogenic carbonate concretion which forms part of the hearing/balance system in fishes. The radial growth of the otolith and the variation of trace elements along the radius appear to capture important aspects of fishes' environmental history [89,90]. Owing to regional and global overfishing, the migration patterns of fish stock are today of highest interest biologically, ecologically and economically. Hence otoliths are being analyzed in several IBA laboratories, including that at Lund, where, in particular, movement of diadromous species (e.g. eel and brown trout) between fresh and brackish water has been determined by analyzing the Sr/Ca ratio [91]. This technique has also been used to identify fish that were raised in freshwater hatcheries and then released into brackish water.

26.4.4 Environmental Studies

Over recent decades there has been extensive use of IBA methods in environmental studies [92, 93]. One reason for this success is probably the very early (1969) use of PIXE for atmospheric samples. Over the three decades following, IBA techniques in combination with many others have had a very important impact on studies of atmospheric aerosols [94], for example in climate change [95] and in urban air pollution [96], and of their regional and industrial impact [97]. The capacity for analyzing many samples for multiple elements in a short time has made PIXE analysis a very important analytical method in these investigations. However, by using microanalytical methods in a nuclear microprobe combined with complementary methods for studying individual aerosol particles, new information can be obtained on the origin of aerosols [98]. In one study, microprobe data were compared with bulk analysis results for large collections of particles [99]. It was estimated that micro-PIXE of aerosols provides data which are accurate to within 10–20%. Possible losses of the elements detected by PIXE in the course of the microprobe bombardment were examined, but were generally found to be insignificant.

26.4.5 Art and Archaeology

One of the best methods for trace element determination in the most sensitive kinds of art and archaeology objects is the use of synchrotron radiation microprobes [100, 101], in which photons produce high characteristic X-ray yields without any significant sample degradation. Nevertheless, the available beam time of such microprobes is very limited, and ion beam analysis, with its complementary capabilities, can be very competitive also for sensitive specimens. The characteristics of ion–matter interaction, however, make it essential to select adequate specimens for a successful and nondestructive investigation of an artefact. On one hand, there are significant changes taking place in an irradiated specimen due to ionization and heating; on the other hand, the external-beam approach can limit these changes to an absolute minimum [102] (see also [6]). This is illustrated by the frequent use of IBA analysis for very sensitive ancient documents. By careful monitoring of the ion beam intensity, it is possible to analyze these precious documents without any visible remaining damage.

The same methods that have been developed within more general materials science are also applicable in this field, as illustrated by [103], where the problem of rapid deterioration due to weathering of stained glass windows in European cathedrals was addressed. The hypothesis was that the rapid deterioration is a result of the airborne pollutants of today. Hence, soda–lime glass samples were exposed to atmospheres in which the temperature, relative humidity and pollutant (SO_2 and NO_2) concentration were systematically varied. After exposure, the surfaces of these glass samples were analyzed using NRA (to profile hydrogen) and RBS.

External-beam PIXE and PIGE have been combined in a study of paint structures in a series of layered paint samples prepared according to known late-18th-century techniques [104]. In a recent study, a group at the University of Florence tried to identify pigments in various paint layers from a painting by Leonardo da Vinci (the "Madonna dei fusi"). By a combination of PIXE and PIGE using external-beam irradiation [105] and corresponding analysis of laboratory-made specimens, it was possible to nondestructively investigate specifically the blue pigments. Since such measurements on very precious artefacts have to be genuinely nondestructive, it is crucial to understand how to avoid formation of "brown spots" on the irradiated surface. A group at the Autonomous University of Madrid carried out such a study on common pigments [106] from natural carbonates. They irradiated the various pigments and used a combination of PIXE and IL to follow the degradation of the material, and then combined it with optical absorption and thermoluminescence to understand the formation of the remaining defects induced. Also, PIXE and RBS have been combined to investigate experimental glazes simulating real painted glazes used as translucent layers on old oil paintings [107].

One serious issue in using IBA methods for the analysis of ancient inhomogeneous artefacts is the superficial preference (the first few to tens of micrometers) of the analytical results. The question is: In a corroded object, how representative are IBA results of the bulk? In order to get around this problem, small spots of objects may be polished mechanically, but then at the risk of changing the exterior and lowering the value of the artefact. As a remedy, a group with long experience of using IBA methods on metallic objects has tried to use controlled laser ablation in conjunction with an external-beam microprobe in a study of thick corrosion layers on archaeological metals [108].

The corrosion process of some materials acts as a protection against further deterioration, and by combining a nuclear microprobe (using PIXE) and XRD (micro-X-ray diffraction) it was possible to investigate the structural composition of this layer in 1500-year-old iron [109]. Phosphate phases in the iron were determined by XRD, and they interfered with oxygen phases in the corrosion process. Although a metallic alloy, for instance bronze, may be essentially free of corrosion, analytical results on trace constituents are not easily obtained, owing to the large presence of heavier elements. Normally PIXE analysis would reveal μg/g concentrations of elements that might be used for provenance studies, but since the detectors are saturated by the signal from major matrix elements, practical detection limits will be much higher. This problem may be circumvented or at least reduced by the use of critical absorbers that reduce the major X-ray lines while preserving the interesting lines [110]. In some metallic specimens, the degree of representation of the bulk and corrosion is less critical but there may instead be a need for combining several methods.

26.5 Conclusions

Being within the more successful fields of application of particle accelerators, ion beam analysis has, together with accelerator-based mass spectrometry (Chap. 23), justified the further development of, in particular, small and medium-size accelerators. As shown in this chapter a great variety of ion beam analysis techniques exists and contributes significantly in many fields of science and technology. There are several other types of IBA applications of great relevance in addition to those presented here. Nevertheless, the applications presented here represent a reasonable display of what can be done with IBA analysis, in particular when making use of high analytical resolution both laterally and in depth. Owing to increasing competition in the analytical arena, it is essential for the future of these techniques that the applications will be even more carefully selected to make full use of the inherent properties of IBA and to combine the techniques with complementary techniques in the most productive manner. The technical developments in accelerators, focusing systems and detector acquisition systems will further ensure and even enhance the potential and success of ion beam analysis techniques.

References

1. N. Nastasi, J.W. Mayer, J.K. Hirvonen: *Ion Solid Interactions: Fundamentals and Applications*, (Cambridge University Press, London 1996)
2. J.R. Tesmer, M. Nastasi, J.C. Barbour, C.J. Maggiore, J.W. Mayer: *Handbook of Modern Ion Beam Materials Analysis* (MRS, Pittsburgh, 1995)
3. J.F. Ziegler: SRIM-2003, available from http://www.srim.org
4. J.A. Maxwell, J.L. Campbell, W.J. Teesdale: Nucl. Instr. Meth. B **43**, 218 (1989)
5. C. Jeynes, N.P. Barradas, P.K. Marriot, G. Boudreault, M. Jenkin, E. Wendler, R.P. Webb: J. Phys D: Appl. Phys. **36**, R97 (2003)
6. P.A. Mandó: Nucl. Instr. Meth. B **85**, 815 (1994)
7. O. Enguita, M.T. Fernández-Jiménez, G. Garcia, A. Climent-Font, T. Calderón, G.W. Grime: Nucl. Instr. Meth. B **219–220**, 384 (2004)
8. R.A. Colman, G.J.F. Legge: Nucl. Instr. Meth. B **73**, 561 (1993)
9. M.B.H. Breese, D.N. Jamieson, P.J.C. King: Microprobe ion optics. In: *Materials Analysis Using a Nuclear Microprobe* (Wiley, New York 1996) pp. 81–139
10. F. Watt, G.W. Grime: *Principles and Applications of High Energy Ion Microprobes*, ed. by M.B.H. Breese, D.N. Jamieson, P.J.C. King (Hilger, Bristol 1987)
11. R. Mimura, H. Takayama, M. Takai: Nucl. Instr. Meth. B **210**, 104 (2003)
12. F. Watt, J.A. van Kan, I. Rajta, A.A. Bettiol, T.F. Choo, M.B.H. Breese, T. Osipowcz: Nucl. Instr. Meth. B **210**, 14 (2003)
13. P. Kristiansson: private communication
14. D. Spemann, T. Reinert, J. Vogt, D. Dobrev, T. Butz: Nucl. Instr. Meth. B **190**, 313 (2002)

15. A. Shariff, P. Kristiansson, V. Auzelyte, M. Elfman, K.G. Malmqvist, C. Nilsson, J. Pallon, M. Wegdén: Nucl. Instr. Meth. B **219–220**, 494 (2004)
16. S.A.E. Johansson, J. Campbell, K.G. Malmqvist: *Particle-Induced X-ray Spectrometry (PIXE)* (Wiley, New York 1995)
17. W. Brandt, G. Lapicki: Phys. Rev. A **20**, 465 (1979)
18. W. Brandt, G. Lapicki: Phys. Rev. A **23**, 1717 (1981)
19. S.I. Salem, S.L. Panossian, R.A. Krause: At. Data Nucl. Data Tables **14**, 91 (1974)
20. J.H. Scofield: Phys. Rev. A **9**, 1041 (1974)
21. J.L. Campbell: Nucl. Instr. Meth. B **31**, 518 (1988)
22. J.H. Scofield: Phys. Rev. A **10**, 1507 (1974)
23. M.H. Chen, B. Crasemann, H. Mark: Phys. Rev. A **24**, 177 (1981)
24. M.H. Chen, B. Crasemann: At. Data Nucl. Data Tables **41**, 257 (1989)
25. H. Paul: Nucl. Instr. Meth. B **3**, 5 (1984); see also erratum in Nucl. Instr. Meth. B **5**, 554 (1984)
26. Y. Miyagawa, S. Nakamura, S. Miyagawa: Nucl. Instr. Meth. B **30**, 115 (1988)
27. F. Folkmann, J. Borggreen, A. Kjeldgaard: Nucl. Instr. Meth. **119**, 117 (1974)
28. K. Ishii, S. Morita: Int. J. PIXE **1**, 1 (1990)
29. L.E. Carlsson, K.R. Akselsson: Nucl. Instr. Meth. **181**, 531 (1981)
30. M. Ahlberg, G. Johansson, K. Malmqvist: Nucl. Instr. Meth. **113**, 377 (1975)
31. W.-K. Chu, J.W. Mayer, M.-A. Nicolet: *Backscattering Spectrometry* (Academic Press, New York 1978)
32. M.R. Weller, M.H. Mendenhall, P.C. Haubert, M. Döbeli, T.A. Tombrello: Heavy ion Rutherford backscattering. In: *High Energy and Heavy Ion Beams in Materials Analysis*, ed. by J.R. Tesmer, C.J. Maggiore, M. Nastasi, J.C. Barbour (MRS, Pittsburgh 1990) pp. 139–151
33. J.A. Knapp, J.C. Banks, B.L. Doyle: Nucl. Instr. Meth. B **85**, 161 (1994)
34. K. Kimura, Y. Oota, K. Nakajima, M. Suzuki: AIP Conf. Proc. **689**, 373 (2002)
35. W.A. Lanford, S. Bedell, S. Amadon, A. Haberl, W., Skala, B. Hjorvarsson: Nucl. Instr. Meth. B **161–163**, 202 (2000)
36. L.R. Doolittle: Nucl. Instr. Meth. B **15**, 227 (1986)
37. A. Seppälä, R. Salonen, J. Slotte, T. Ahlgren, E. Rauhala, J. Räisänen: Nucl. Instr. Meth. B **161–163**, 520 (2000)
38. R. Samlenski, C. Haug, R. Delto, C. Wild, R. Brenn: Nucl. Instr. Meth. B **190**, 324 (2002)
39. R. Groleau, S.C. Gujrathi, J.P. Martin: Nucl. Instr. Meth. **218**, 11 (1983)
40. R. Ishigami, Y. Ito, K. Yasuda, M. Sasase, S. Hatori: AIP Conf. Proc. **689**, 474 (2002)
41. R. Siegele, I. Orlic, D.D. Cohen: Nucl. Instr. Meth. B **190**, 301 (2002)
42. H.J. Whitlow: Mass and energy dispersive recoil spectrometry: a new quantitative depth profiling technique for microelectronic technology. In: *High Energy and Heavy Ion Beams in Materials Analysis*, ed. by J.R. Tesmer, C.J. Maggiore, M. Nastasi, J.C. Barbour (MRS, Pittsburgh 1990) pp. 73–85
43. G. Vizkelethy: Nuclear reaction analysis: particle–particle reactions. In: *Handbook of Modern Ion Beam Material Analysis*, ed. by J.R. Tesmer, M. Nastar et al. (MRS, Pittsburgh 1995) Chap. 6
44. D. Dieumegard, B. Maurel, G. Amsel: Nucl. Instr. Meth. **168**, 93 (1980)
45. R.A. Jarjis: Nuclear cross-section data for surface analysis Vols. I–III, University of Manchester report (1979)

46. A.K.M. Fazlul Hoque, M. Khaliquzzaman, M.D. Hssain, A.H. Khan: Fluoride **35**, 176 (2002)
47. N.M. Uzunov, I.P. Penev, A.M. Artinian: Nucl. Instr. Meth. B **95**, 276 (1995)
48. J. Räisänen: Nucl. Instr. Meth. B **40/41**, 638 (1989)
49. A. Anttila, R. Hänninen, J. Räisänen: J. Radioanal. Chem. **62**, 441 (1981)
50. I. Giles, M. Peisach: J. Radioanal. Chem. **50**, 307 (1979)
51. J. Pallon, V. Auzelyte, M. Elfman, M. Garmer, P. Kristiansson, K.G. Malmqvist, C. Nilsson, A. Shariff, M. Wegdén: Nucl. Instr. Meth. B **219–220**, 988 (2004)
52. G. Devés, R. Ortega: Anal. Bioanal. Chem. **374**, 390 (2002)
53. M.B.H. Breese, D.N. Jamieson, P.J.C. King (eds.): Spatially resolved ion channelling techniques. In: *Materials Analysis Using a Nuclear Microprobe* (Wiley, New York 1996) pp. 201–246
54. H.W. Lefevre, R.M.S. Schofield, D.R. Ciarlo: Nucl. Instr. Meth. B **54**, 47 (1991)
55. G.S. Bench, K.A. Nugent, M. Cholewa, A. Saint, G.J.F. Legge: Nucl. Instr. Meth. B **54**, 390 (1991)
56. D. Habermann: Mineral. Petrol. **76**, 247 (2002)
57. C. Yang, N.P.-O. Homman, K.G. Malmqvist, L. Johansson, N.M. Halden, V. Barbin: Scanning Microsc. **9**, 43 (1995)
58. K.G. Malmqvist, M. Elfman, G. Remond, C. Yang: Nucl. Instr. Meth. B **109/110**, 227 (1996)
59. C. Yang, K.G. Malmqvist, M. Elfman, P. Kristiansson, J. Pallon, A. Sjöland, R.J. Utui: Nucl. Instr. Meth. B **130**, 746 (1997)
60. G. Vizkelethy, F.O. McDaniel, S. Thevuthasan, J.R. Tesmer: Nucl. Instr. Meth. B **219–220**, (2004)
61. N. Matsumura, T. Haga, S. Muto, Y. Nakata, N. Yokohama, K. Numata, K. Yabuta: Physica E **13**, 1168 (2002)
62. F. Watt, I. Rajta, J.A. Van Kan, A.A. Bettiol, T. Osipowicz: Nucl. Instr. Meth. B **190**, 306 (2002)
63. L. Wei: Mater. Res. Soc. Symp. Proc. **721**, 105 (2002)
64. L. Wei: AIP Conf. Proc. **689**, 464 (2002)
65. T. Osipowicz, H.L. Seng, L.S. Wielunski, E.S. Tok, G. Breton, J. Zhang: Nucl. Instr. Meth. B **190**, 345 (2002)
66. E.J. Teo, M. Alkaisi, A.A. Bettiol, T. Osipowicz, J. Van Kan, F. Watt, A. Markwitz: Nucl. Instr. Meth. B **190**, 339 (2002)
67. G. Amsel, G. Battistig, A. L'Hoir: Nucl. Instr. Meth. B **201**, 325 (2003)
68. N. Kawachi, T. Katabuchi, M. Yamaguchi, Y. Tagishi: Nucl. Instr. Meth. B **190**, 195 (2002)
69. P. Kristiansson, T. Larsson, S. Malmberg, L. Malmqvist, K. Malmqvist, M. Elfman, J. Pallon: Nucl. Instr Meth. B **158**, 665 (1999)
70. P. Kristiansson, M. Elfman, T. Larsson, S. Malmberg, L. Malmqvist: Ink distribution on newsprints with high and low smearing, Proc. 1998 International Printing and Graphic Art Conference, Quebec
71. K.-E. Saarela, L. Harju, J.-O. Lill, J. Rajander, A. Lindroos, S.-J. Heselius, K. Saari: Holzforschung **56**, 380 (2002)
72. H. Khodja, E. Berthoumieux, L. Daudin, J.-P. Gallien: Nucl. Instr Meth. B **181**, 83 (2001)
73. H. Yamazaki, Y. Takahashi, K. Ishii, S. Matsuyama, T. Satoh, H. Orihara: J. Nucl. Sci. Tech. Suppl. **3**, 560 (2002)

74. U. Alonso, T. Missana, A. Patelli, V. Rigato, P. Rivas: J. Contam. Hydrol. **61**, 95 (2003)
75. C.G. Ryan: Nucl. Instr. Meth. B **104**, 377 (1995)
76. C.G. Ryan, D.N. Jamieson, W.L. Griffin, G. Cripps, R. Szymanski: Nucl. Instr. Meth. B **181**, 12 (2001)
77. D.D. Hickmott, J. Stimac, A.C.L. Larocque, C. Wettland, A. Brearly: AIP Conf. Proc. **689**, 440 (2002)
78. L.J. Cabri, P.J. Sylvester, M.N. Tubrett, A. Peregoedova, J.H.G. LaFlamme: Can. Mineral. **41**, 321 (2003)
79. P. Kristiansson, U. Hålenius, H. Skogby, M. Elfman, K.G. Malmqvist, J. Pallon: Nucl. Instr. Meth. B **158**, 562 (1999)
80. M. Volfinger: J. Radional. Nucl. Chem. **253**, 413 (2002)
81. L. Malmqvist, K. Kristiansson, P. Kristiansson: Nucl. Instr. Meth. B **150**, 484 (1999)
82. C.A. Pineda-Vargas, A.L. Rodgers, M.E. Eisa: Radiat. Phys. Chem. **71**, 947 (2004)
83. W.J. Przybylowicz, J. Mesjasz Przybylowicz, P. Migula, E. Glowacka, M. Nakonieczny, M. Augustyniak: Nucl. Instr. Meth. B **210**, 343 (2003)
84. J. Pallon, M. Elfman, P. Kristiansson, K. Malmqvist, E. Graneli, A. Sellborn, C. Karlsson: Nucl. Instr. Meth. B **158**, 312 (1998)
85. R. Ortega, A. Suda, E. GeVes: Nucl. Instr. Meth. B **210**, 364 (2003)
86. M. Wegdén, P. Kristiansson, C. Ceberg, P. Munck af Rosenschöld, V. Auzelyte, M. Elfman, K.G. Malmqvist, C. Nilsson, J. Pallon, A. Shariff: Nucl. Instr. Meth. B **219–220**, 67 (2004)
87. W.J. Przybylowicz, J. Mesjasz-Przybylowicz, V.M. Prozesky, C.A. Pineda: Nucl. Instr. Meth. B **130**, 335 (1997)
88. D. Budka, J. Mesjasz-Brzybylowicz, W.J. Brzybylowicz: Radiat. Phys. Chem. **71**, 785 (2004)
89. G.E. Coote, R.W. Gauldie, I.F. West: Nucl. Instr. Meth. B **54**, 144 (1991)
90. J.L. Campbell, J.A. Babaluk, N.M. Halden, A.H. Kristofferson, J.A. Maxwell, S.R. Mejia, J.D. Reist, W.J. Teesdale: Nucl. Instr. Meth. B **150**, 260 (1999)
91. M. Elfman, K.E. Limburg, P. Kristiansson, K. Malmqvist, J. Pallon: Nucl. Instr. Meth. B **150**, 272 (1999)
92. K.G. Malmqvist: Nucl. Instr. Meth. B **85**, 84 (1994)
93. K.G. Malmqvist: Nucl. Instr. Meth. B **113**, 336 (1996)
94. E. Swietlicki, B.G. Martinsson, P. Kristiansson: Nucl. Instr. Meth. B **109/110**, 385 (1996)
95. T.A. Cahill: Nucl. Instr. Meth. B **109/110**, 402 (1996)
96. F. Lucarelli, P.A. Mando, S. Nava, P. Prati, A. Zucchiatti: Nucl. Instr. Meth. B **161/163**, 819 (2000)
97. D.D. Cohen, E. Stelcer, D. Garton: Nucl. Instr. Meth. B **190**, 466 (2002)
98. E. Perdrix, G. Lecornet, P. Delain, S. Sobanska, H. Guegan, J. Laureyns, A. Robache, A. Morin: J. Phys. **107**, 1037 (2003)
99. W. Maenhaut, R. Salomonovic, J. Ptasinski, G.W. Grime: Nucl. Instr. Meth. B **130**, 576 (1997)
100. E. Dooryhée, P. Martinetto, Ph. Walter, M. Anne: Radiat. Phys. Chem. **71**, 863 (2004)
101. P.M. O'Neill, D.C. Creagh, M. Sterns: Radiat. Phys. Chem. **71**, 841 (2004)
102. J. Absil, H.-P. Garnir, D. Strivay, C. Oger, G. Weber: Nucl. Instr. Meth. B **198**, 90 (2002)

103. K. Cummings, W.A. Lanford, M. Feldmann: Nucl. Instr. Meth. B **136/138**, 858 (1998)
104. J.-O. Lill, M. Ström, M. Brenner, A. Lindroos: Nucl. Instr. Meth. B **189**, 303 (2002)
105. N. Grassi, A. Migliori, P.A. Mandó, H. Calvo, H. Calvo de Castillo: Nucl. Instr. Meth. B **219–220**, 48 (2004)
106. O. Enguita, T. Calderon, M.T. Fernandez-Jimenez, P. Beneitez, A. Millan, G. Garcia: Nucl. Instr. Meth. B **219–220**, 53 (2004)
107. L. Simonot, A. Zobelli, M. Elias, J. Salomn, J.C. Dran: J. Trace Microprobe Tech. **21**, 35 (2003)
108. M.H. Abraham, G.W. Grime, M.A. Marsh, J.P. Northover: Nucl. Instr. Meth. B **180**, 688 (2001)
109. P. Dillman, R. Balasubramaniam, G. Beranger: Corrosion Sci. **44**, 2331 (2002)
110. K. Morito, S. Nagashima, M. Kato, T. Kotani, M. Uda: Nucl. Instr. Meth. B **109/110**, 569 (1996)